RSC Advances

ROYAL SOCIETY OF CHEMISTRY

www.rsc.org/advances

Solid-state-reaction synthesis of VO_2 nanoparticles with low phase transition temperature, enhanced chemical stability and excellent thermochromic properties

Nan Shen,[1,3] Bingrong Dong,[1,3] Chuanxiang Cao,[1] Zhang Chen[2], Hongjie Luo,[1,2] Yanfeng Gao,[1,2]*

1.Shanghai Institute of Ceramics (SIC), Chinese Academy of Sciences (CAS), No. 1295 Dingxi Road, Changning District, Shanghai, 200050, China
2.School of Materials Science and Engineering, Shanghai University, No. 99 Shangda Road, Shanghai, 200444, China
3. University of Chinese Academy of Sciences, Beijing, 100049, China

* Author for correspondence. Yanfeng Gao, Shanghai University,
Email: yfgao@shu.edu.cn Tel/Fax: +86-21-6613-8005

Abstract

Synthesis of VO_2 has been a fundamental topic in the study of VO_2-based materials for energy-saving applications. Methods including hydrothermal, sol-gel and chemical vapor deposition can be used to synthesize VO_2 (M1/R). However, these techniques may usually involve some problems such as expensive raw materials, complex steps, and difficulties in controlling appropriate ratios of precursor amounts. In this study, a solid-state-reaction route was developed to prepare well-crystallized VO_2 (M1/R) nanoparticles with low, variable phase transition temperature, enhanced chemical stability and excellent thermochromic properties. The phase transition temperatures ranged from 43.5 ℃ to 59.3 ℃ by regulating reaction conditions, and it could be inferred from the study of the preparation process that the amorphous phases around the crystalline VO_2 phases played an important role in the decrease of phase transition temperatures compared with the reported values for bulk VO_2 (68 ℃). Moreover, the obtained VO_2 (M1/R) nanoparticles exhibited enhanced anti-oxidation and acid-resistance abilities compared with particles prepared by hydrothermal process, and the derived flexible foils on polymer from the prepared VO_2 (M1/R) nanoparticles showed excellent thermochromic properties (T_{lum} =54.2 % , ΔT_{sol} =9.2 %).

Keywords: VO_2 (M1/R) nanoparticle, synthesis, solid-state reaction, thermochromic property

Introduction

Vanadium dioxide (Monoclinic/Rutile phase, denoted as M1/R) has attracted significant attention for its reversible metal-semiconductor phase transition (MST) accompanied with a structural transformation from low-temperature insulating monoclinic phase ($P2_1/c$, M1) to high-temperature metallic rutile phase ($P4_2/mnm$, R) at a critical temperature (T_c) of 68 °C. Across the MST, VO_2 exhibits a sharp change in the infrared optical transparency and electric resistivity within ultrafast time horizons (several ps). These unique characteristics make VO_2 be widely used in ultrafast optical switches[1, 2], optical storage devices[3], field effect transistors[4], and smart window applications[5-7].

The synthesis of VO_2 (M1/R) has long been a research focus since VO_2 (M1/R) was first found. To date, many approaches have been investigated to prepare VO_2 (M1/R), which could mainly be classified into two categories: gas-phase methods and solution-based processes. Gas-phase techniques such as chemical vapour deposition (CVD)[8, 9], pulsed laser deposition (PLD)[10, 11], and sputtering deposition[12-14] have been explored to fabricate VO_2 (M1/R) films, which shows advantages in precisely controlling the oxygen partial pressure[15, 16] and successfully preparing well-crystallized films with many distinctive nano-structures[17, 18]. The sol-gel process[19, 20] and polymer-assisted deposition method[21] have been developed to prepare VO_2 (M1/R) films with low cost, but specific raw materials such as polymers are commonly needed, which significantly limits practical uses. Alternatively, hydrothermal methods[22-24] have been used to synthesize VO_2 (M1/R) nanoparticles (denoted as NPs), which could subsequently be dispersed into polymer matrix to prepare VO_2 (M1/R) nano-composite foils[25-28] with excellent thermochromic properties. However, many present studies are still involved in a two-step method[29, 30], of which VO_2 intermediate phases (such as VO_2 (B)) are prepared first and then they are transformed into VO_2 (M1/R) by post annealing treatment. Moreover, VO_2 (M1/R) NPs obtained by hydrothermal methods may be confronted with problems of high phase transition temperature, chemical instability and low luminous transmittance,

which restricts their application scope in various fields.

Up to now, solid-state reaction has barely been used to synthesize VO_2 (M1/R) NPs. Previously, Wu et al[31] successfully prepared VO_2 (M1/R) NPs through a structure-conversion pathway from goethite VOOH to paramontroseite VO_2 to rutile VO_2(R), of which each of two steps was only required within 60 s. However, more detailed information of properties based on solid-state reaction was not revealed.

In this study, we proposed a solid-state-reaction route to prepare well-crystallized VO_2 (M1/R) NPs with low, variable phase transition temperature, enhanced chemical stability and excellent thermochromic properties. The phase transition temperatures ranged from 43.5 °C to 59.3 °C under different reaction conditions, and the existence of amorphous phases around the crystalline VO_2 phases is probably accounted for lower phase transition temperatures than the reported values (68°C). Moreover, the obtained VO_2 (M1/R) NPs exhibited enhanced anti-oxidation and acid-resistance abilities compared with particles prepared by hydrothermal process, and the derived foils from the prepared VO_2 (M1/R) NPs showed excellent thermochromic properties (T_{lum} = 54.2 % , ΔT_{sol} =9.2 %).

2 Experiment and Characterization

2.1 Preparation of VO_2 (M1/R) nanoparticles

All reagents were of analytical grade and were used without further purification. In a typical procedure, 0.125 g V_2O_5 powders were added into 40 mL of 0.15 M aqueous $H_2C_2O_4 \cdot 2H_2O$ to form a clear VO^{2+} solution and the solution was stirred for 30 min. The pH value of the resultant solution was adjusted to 7 by using moderate amount of sodium hydroxide solution (0.1 M). A brown precursor formed during the addition of sodium hydroxide. The precursor was collected, washed with 30 mL of deionised water and then dried in a vacuum oven. In order to obtain VO_2 (M1/R) NPs, the precursor powders were set in a nitrogen-filled furnace to undergo the solid-state reaction at 350 ~ 600 ºC for different reaction times. The final product was collected, washed three times with deionized water and dried in a vacuum oven at 60 °C for 12 h. The hydrothermally synthesized nanoparticles employed for comparable study of

chemical stability were prepared according to the following steps.[27] 0.125 g V_2O_5 powder were added into 40 mL of 0.15 M aqueous $H_2C_2O_4 \cdot 2H_2O$ to form a yellowish slurry. The slurry was stirred for 10 min and transferred to a 50 mL Teflon-lined stainless-steel autoclave. The autoclave was maintained at 260 ºC for 24 h and then air-cooled to room temperature. The final product was collected via centrifugation, washing three times with deionized water and drying in a vacuum oven at 60 ºC for 12 h.

2.2 Preparation of VO_2/PU composite foil

The VO_2-polyurethane (PU) thermochromic composite foils were prepared according to the following step.[7, 32] The as-prepared VO_2 (M1/R) NPs were dispersed in deionised water with continuous stirring for 10 min and a suitable quantity (one fiftieth of water amount, in volume) of the silane coupling agent KH-570 was added with ultrasonic treatment for approximately 30 min. Then, PU ($(C_{10}H_8N_2O_2 \cdot C_6H_{14}O_3)_n$, DISPERCOLL U54, Bayer) was gradually added along with stirring about 20 min. Finally, the suspension was uniformly cast onto a polyethylene terephthalate (PET) substrate using an automatic coating machine and dried at 80 ℃ for 1 min.

2.3 Characterizations and Calculation

The morphology and element composition of the resulting powders were analysed via transmission electron microscopy (TEM, JEM2010, JEOL, Japan) with an energy-dispersive spectrometer (EDS) attachment. The crystalline structures of the resultant products were characterized with a Rigaku D/max 2550V X-ray diffractometer (Japan) with Cu Kα radiation (λ = 0.15406 nm). X-ray photoelectron spectrometry (XPS) was performed with an Axis ultra DLD instrument using monochromatic Al Kα radiation after 1 keV argon-ion etching for 10 s. The phase transition temperatures of the products were measured via differential scanning calorimetry (DSC, DSC200F3, NETZSCH) in nitrogen flow in the temperature range from 0 °C to 100 °C at a heating rate of 10 °C min^{-1}. The spectrum characteristics of the VO_2-PU composite foils were monitored in the range of 240-2600 nm on a Hitachi

U-4100 UV visible-near-IR spectrophotometer equipped with a film heating unit.

For all samples, the integral luminous transmittance (T_{lum}, 380-780 nm) and solar transmittance (T_{sol}, 240-2600 nm) were obtained based on the measured spectra using the following equation:

$$T_i = \int \varphi_i(\lambda) T(\lambda) d\lambda / \int \varphi_i(\lambda) d\lambda \quad (1)$$

$$\Delta T_{sol} = T_{sol}(T < T_c) - T_{sol}(T > T_c) \quad (2)$$

where $T(\lambda)$ denotes the transmittance at wavelength λ, i denotes 'lum', or 'sol' for the calculations, T and ΔT_{sol} are the temperature and solar energy modulation ability, φ_{lum} is the standard luminous efficiency function for the photopic vision (shown in Figure S3 with deep grey colour), and φ_{sol} are the solar irradiance spectrum (shown in Figure S3 with light grey colour) for air mass 1.5 (corresponding to the sun standing 37° above the horizon).

3 Results and discussion

3.1 The synthesis of VO_2 (M1/R) nanoparticles

The synthesis of VO_2 nanoparticles via solid-state-reaction underwent decomposition and nucleation from precursors according to previous research[5,25]. The precursor[5,25,26] is an amorphous phase, which was confirmed in current study (with XRD pattern in Figure S1). As shown in Figure 1a, the decomposition reaction of precursor occurred at approximate 250 ºC, and VO_2 (R) started to nucleate at 343 ºC. The formation of VO_2 (M1/R) was considered to occur as follows:

$$x{\cdot}VO(OH)_2 \xrightarrow{250\ ^oC} V_xO_{2x} \xrightarrow{343\ ^oC} (VO_2)_x\,(R)$$

The XRD patterns in Figure 1 show that all the peaks for the VO_2 nanoparticles could be indexed to VO_2 (M1) phase (JCPDS card No. 72-0514) and no other phases were detected. Due to the nucleation of VO_2 (R) at 343 ºC (Figure 1a), the reaction temperature should set higher than that value. And it could be observed that the x-ray diffraction intensity of VO_2 (M1/R) formed at 350 ºC for 1 h was rather poor (Figure 1b). As the reaction temperature increased from 350 ºC to 600 ºC, the intensity of the

diffraction peaks significantly enhanced (Figure 1b), indicating a great improvement of the crystallinity. Similarly, the intensity of the diffraction peaks gradually increased as the reaction time was prolonged from 1h to 15h at 500 ºC (Figure 1d). Thus, one can learn that prolonging the reaction time at low temperature (350 ºC -10h, Figure 1c) and raising the heating temperature (600 ºC -1h, Figure 1b) for short reaction time both could improve the crystallinity of VO_2 nanoparticles. It could also be observed that the width of the diffraction peaks narrowed with the peak intensity enhancing (Figure 1b-d), indirectly showing the growth of VO_2 (M1/R) NPs.

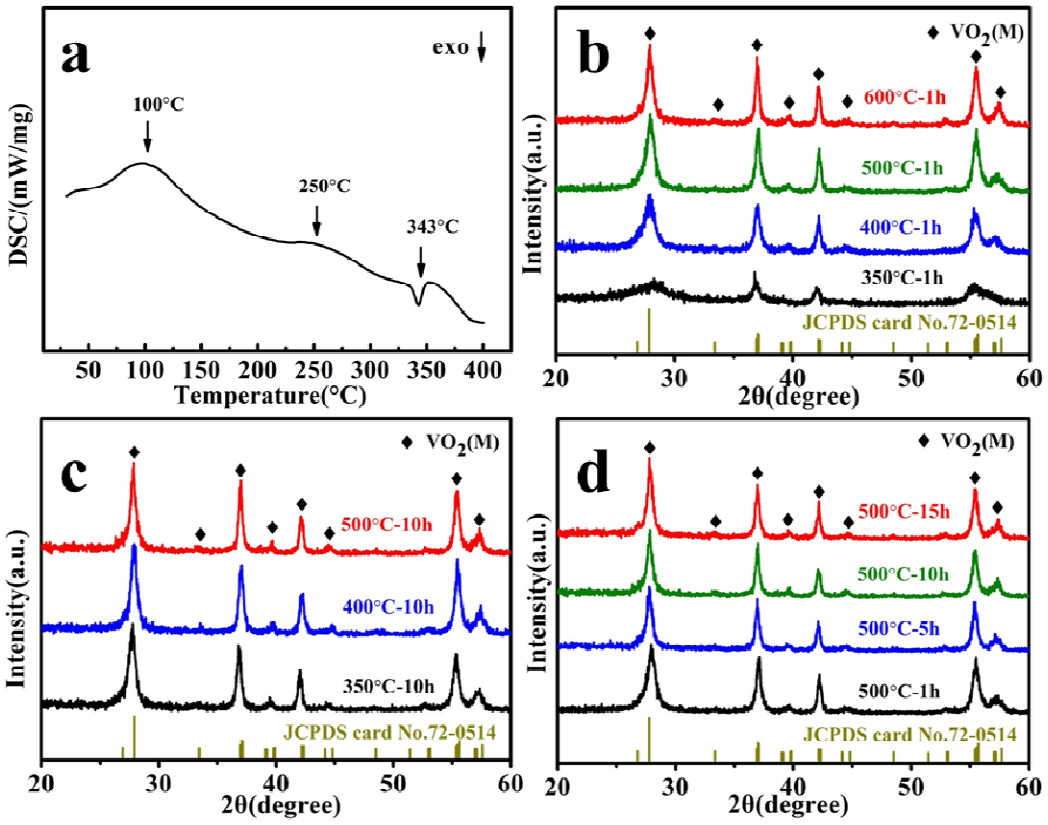

Figure 1 (a) The DSC results of precursor. The XRD patterns of samples obtained at different reaction temperatures for (b) 1h, and (c) 10h. (d) The XRD patterns of samples obtained for different reaction times at 500 ºC.

X-ray photoelectron spectroscopy (XPS) of as-obtained VO_2 (M1/R) NPs was described in Figure 2d. The binding energy of the $V2p_{3/2}$ peaks centered at 516.2 eV (Figure 2d) was in good agreement with 516.0 eV of pure VO_2.[33] The difference in the binding energy between O1s and $V2p_{3/2}$ was 14.0 eV, corresponding to that value of

literature (14.2 eV).[21] Combined with XRD, the data of XPS provided an effective evidence of no other vanadium valences in VO_2 (M1).

The morphology of the VO_2 (M1/R) NPs was studied by SEM (Figure 2a) and TEM (Figure 2c), which showed the spherical appearance of VO_2 (M1/R) NPs. Selected area electron diffraction (SAED) patterns (the inset in Figure 2c) revealed that the VO_2 NPs could be indexed to VO_2 (M1), which was consistent with XRD patterns. Moreover, the EDS results (Figure 2b) further confirmed that there was no other impurity in the VO_2 (M1/R) NPs.

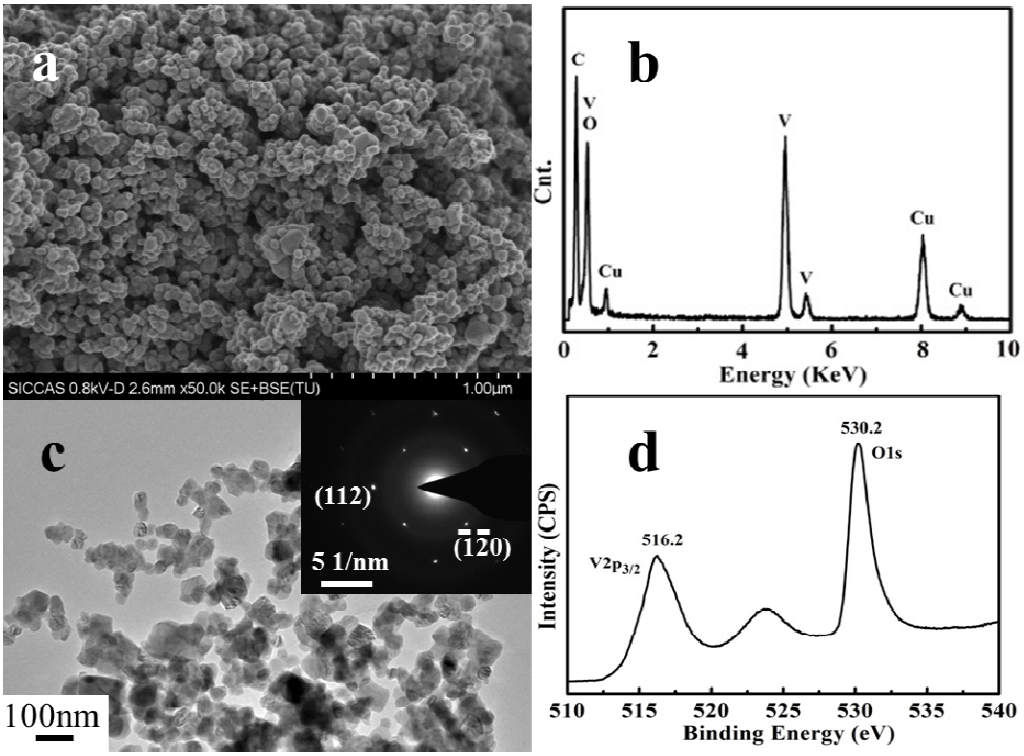

Figure 2 The FESEM image (a), EDS results (b), TEM graph (c, inset: SAED pattern) and core level spectra of V2p (d) of VO_2 samples obtained by reaction maintained at 500 ºC with 15h.

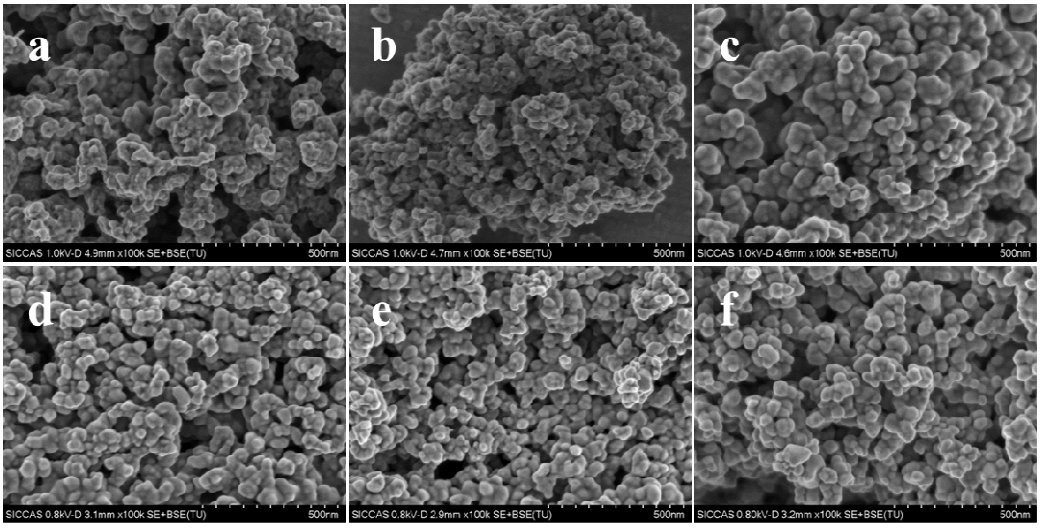

Figure 3 SEM photos of VO_2 samples : (a) 350ºC-1h, (b) 400ºC-1h, (c) 500ºC-1h, (d) 350ºC-10h, (e) 400ºC-10h, (f) 500ºC-10h

In order to systematically investigate the growth of VO_2 (M1/R) NPs in the solid-state reaction process, the morphology evolution was studied at different temperatures with different times. Since VO_2 (R) started to nucleate at 343 ºC (Figure 1a), the reaction temperature was better to be set above 350ºC (Figure 1b). When the reaction was maintained at 350ºC for 1 h, VO_2 (R) phase was generated (Figure 1b) but VO_2 (M1/R) NPs stuck to each other with poor crystallinity, which could be observed from the SEM graphs (Figure 3a). The crystallinity of VO_2 (M1/R) NPs was gradually improved (Figure 3c) with more distinct grain boundary when the reaction temperature was increased to 500 ºC, and a more obvious enhancement of crystallinity could also be achieved by extending the reaction time from 1h to 10h (Figure 3d-f).

From Figure 1b, it could be inferred that 500 ºC was an appropriate temperature to specifically observe the growth evolution of VO_2 (M1/R) NPs with gradually prolonging the reaction time. Annealing for 1 h, VO_2 (M1/R) NPs were partly formed, but there existed enormous amorphous phases around the VO_2 (M1/R) NPs. Tight adhesion could also be observed among adjacent nanoparticles and the sizes of these initially nucleated nanoparticles were quite small. Extending time to 5 h, the VO_2 (M1/R) NPs grew gradually and the amorphous phase decreased obviously (Figure 4b); grain boundaries were rather clear. Further prolonging to 10 h, merging between

adjacent grains occurred (Figure 4c) and the NPs became significantly large after 15 h (Figure 4d). Besides, the average size of VO_2 (M1/R) NPs increased from 29 nm to 72 nm as the reaction time was extended (Figure 4).

The similar morphology evolution from amorphous vanadium oxides to crystallized VO_2 (M1/R) phase could also be further confirmed by TEM and HRTEM images (Figure 5). As shown in Figure 5a and 5d, there was still a certain amount of amorphous substances around the VO_2 (M1/R) NPs at 5h. Till 10h, these non-crystalline matters were further diminished to a large extent (Figure 5b and 5e), and were finally transformed at 15 h (Figure 5c and 5f), exhibiting the same change as Figure 4.

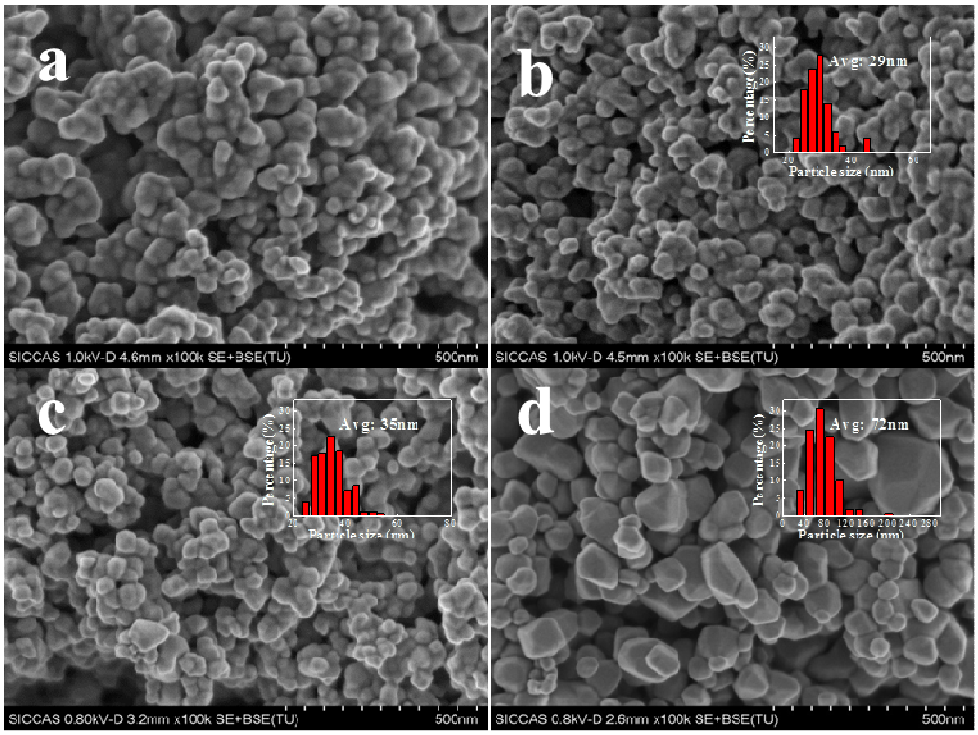

Figure 4 SEM photos of VO_2 samples obtained at 500 ºC for different reaction times: (a) 1 h, (b) 5 h, (c) 10 h, (d) 15 h. Insets in (b),(c) and (d) show the particle size distribution counted from 150 particles.

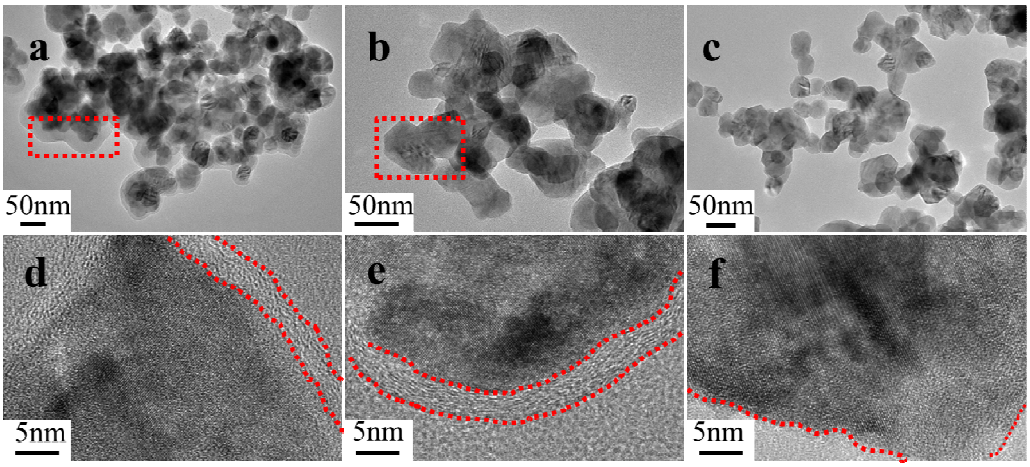

Figure 5 TEM photos and HRTEM images of VO_2 samples obtained at 500 ºC for different reaction times, 5 h: (a) and (d), 10 h :(b) and (e), 15 h: (c) and (f)

3.2 The phase transition property of VO_2 (M1/R) nanoparticles

The phase transition temperature (T_c for semiconductor-metal transition, SMT) determines the energy-saving performance of VO_2-based smart windows[25,27,28], and the value of T_c should be as close as room temperature to achieve excellent energy-saving performance. And the latent heat of the phase transition reflects the thermochromic properties of VO_2 nanoparticles[26], almost corresponding to the value of solar energy modulation ability of the VO_2-nanoparticle-derived foils[27]. As shown in Figure 6a (in which the endothermic peak corresponds to the semiconductor-metal transition), the T_c (43.5 ºC) of VO_2 (M1/R) NPs at 1h was much lower than the reported T_c (68 ºC)[34] of undoped VO_2, and meanwhile the latent heat of the phase transition was quite small (about 3.3 J/g), indicating the poor crystallinity of samples obtained at low temperature (350 ºC-1 h). By contrast, the T_c and latent heat were both enhanced obviously for 10 h (Figure 6b). It could also be observed that raising the reaction temperature was beneficial to the increase of T_c and latent heat (Figure 6a and 6b), especially for the samples obtained for the short reaction time (Figure 6a).

Specifically, the influence of reaction time on the phase transition properties was further studied. As shown in Figure 6c, the T_c of VO_2 (M1/R) NPs obtained at 500 ºC ranged from 49.5 ºC to 59.3 ºC with the reaction time varying from 1 h to 15 h. And the latent heat of the phase transition (Figure 6d) demonstrated a increasing trend with initially large and then slow rate as the reaction time prolonged. Since the crystallinity

reflects the latent heat of MST in undoped VO_2 system, the increase of latent heat (Figure 6d) indirectly verified the improvement of the crystallinity, which was consistent with the results in Figure 5.

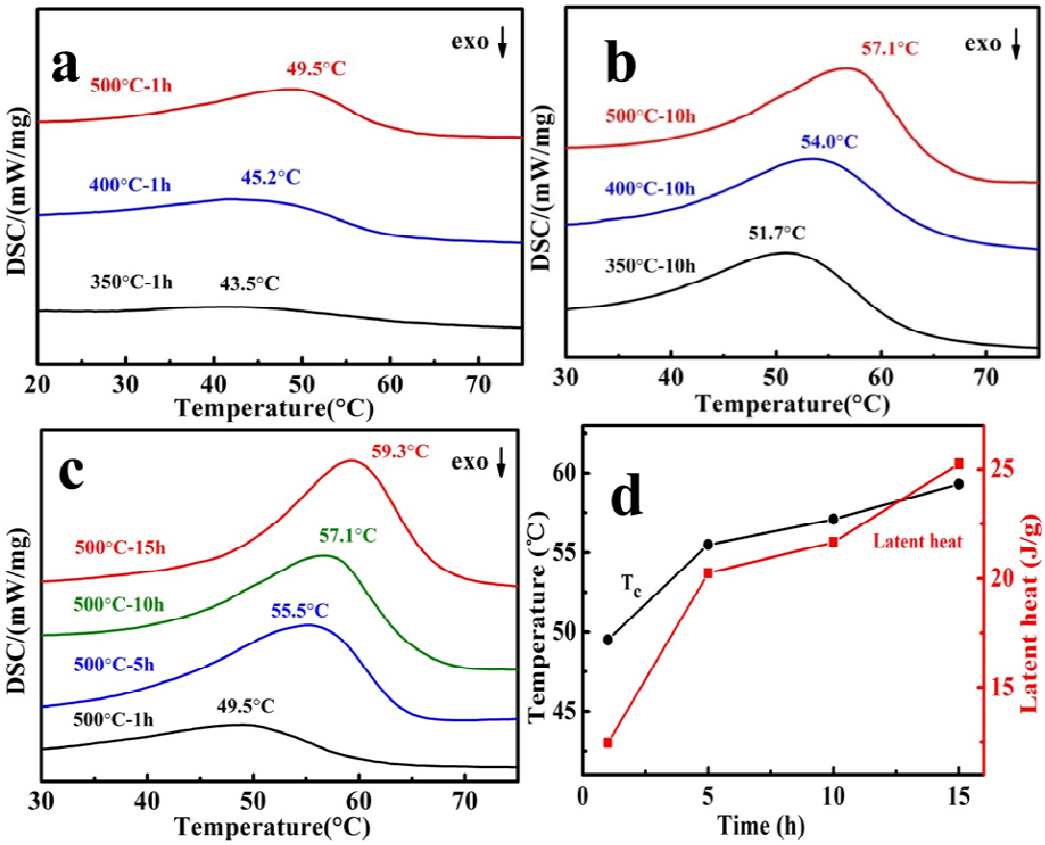

Figure 6 The phase transition properties of VO_2 samples. (a) The DSC curves of samples obtained at different reaction temperatures for 1h. (b) The DSC curves of samples obtained at different reaction temperatures for 10h. (c) The DSC curves of samples obtained for different reaction times at 500 ºC. (d) The phase transition temperatures and latent heat values of VO_2 samples obtained for different reaction times at 500 ºC

As previous research proved, the phase transition temperature of VO_2 (M1/R) can be regulated by metal element doping[28, 35], stress designing[36], defects engineering[30], size effect[37] and non-stoichiometry[38]. The SMT temperature decrease in this work could be ascribed to a combination of a series of factors including defect, size effects, stress and non-stoichiometry due to the complexity of the NPs surrounded by amorphous substances. To make the above factors more clearly, the NPs were analyzed below. XPS measurements of the O1s and V2p (Figure S2)

showed that there was no significant changes of valence state for the samples obtained at different reaction conditions. Vanadium in all samples only exhibited +4 valence state (with a binding energy of 516.0 eV[33]), which excluded the effect of non-stoichiometry on the phase transition temperature. As for stress, it could be related to the phase transition temperature due to the amorphous substance around the nanoparticles, which was similar to the VO_2-SiO_2 core-shell structure in our previous work[32]. From Figure 4, a size increase of VO_2 (M1/R) NPs could be observed with extending the reaction time, however, the size effect may be not the sole reason for T_c increase according to previous studies[25,30]. Combined with the investigation of morphology evolution, it was probable that the amorphous substances around the VO_2 (M1/R) NPs (observed from Figure 4 and Figure 5) played an important role in the lower T_c,[32] since the poor crystallized parts (within the red dashed line region in Figure 5) might involve massive defects such as oxygen vacancies, dislocations and other structural imperfections[39]. Therefore, it could be ideally anticipated that the T_c would ultimately be enhanced to the reported value only if the reaction time is set long enough (such as more than 20 h) or the reaction temperature is high enough to reduce the defects.

3.3 The thermochromic properties of VO_2-PU foils

The UV-Vis-NIR transmittance spectra (Figure 7) of the VO_2-PU foils were obtained at 25 ºC and 90 ºC, respectively. The integral luminous transmittance (T_{lum}) and the solar energy modulation ability (ΔT_{sol}) were calculated according to the method described in Section 2.3. From Figure 7 and table 1, one can see that the integral luminous transmittance (T_{lum}) of sample I at 25 ºC was 56.3 %, much higher than the values (45.3%)[28] of undoped VO_2 (M1/R) prepared by hydrothermal method, and the solar energy modulation ability (ΔT_{sol}) was 7.3 %, much lower than the excellent performance (22.3 %)[25]. As the reaction temperature increased (Table 1: I, II, IV), T_{lum} gradually decreased to 43.7 % as a result of the growth of nanoparticles (Figure 3). Meanwhile, due to the improvement of crystallinity, ΔT_{sol} was enhanced correspondingly. Moreover, with the reaction time prolonging (Table 1: III to V), the T_{lum} was reduced from 46.3 % to 39.3 % but ΔT_{sol} increased from 8.2 % to 10.5 %,

close to most of reported values of present research[40]. Although the ΔT_{sol} seems rather lower than the excellent value (22.3 %)[25], various attempts could be combined with the synthesis process to improve ΔT_{sol} as well as the T_{lum}, such as elemental doping[26, 27] and growth control of nanoparticles[25].

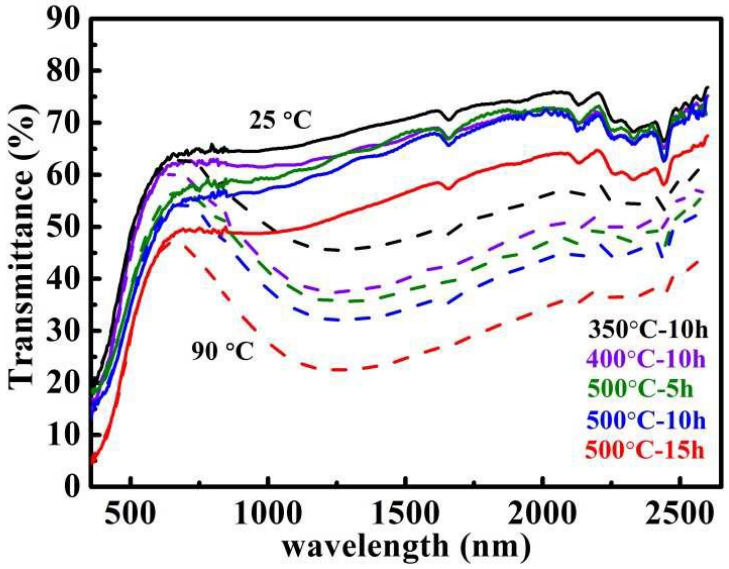

Figure 7 The optical properties of VO_2 samples

Table 1 The integral luminous transmittance (T_{lum}) and solar energy modulation ability (ΔT_{sol}) of VO_2 samples obtained at different conditions

sample	T_{lum} (%)		ΔT_{sol} (%)
	25 ℃	90 ℃	
I (350°C-10h)	56.3	56.1	7.3
II (400°C-10h)	54.2	53.7	9.2
III (500°C-5h)	46.3	47.6	8.2
IV (500°C-10h)	43.7	44.9	9.0
V (500°C-15h)	39.3	39.1	10.5

3.4 Chemical stability property of VO_2 (M1/R) nanoparticles

Since VO_2 was reported to be gradually oxidized into V_2O_5 when it is exposed in air for a long period (such as six months[20]) or placed in the presence of oxygen at high temperature above 300 °C [41, 42], a comparative study of VO_2 (M1/R) NPs after heat

treatment at 300 ℃ in air was shown in Figure 8. It could be seen that the hydrothermal sample (Figure 8a) was almost completely transformed to V_2O_5 in 30 min, while the sample (400 ℃ -10h) in this work was partially transformed to V_2O_5 (Figure 8b), and the other sample (500 ℃ -10h) (Figure 8c) was just slightly oxidized, indicating that the VO_2 (M1/R) NPs in this work exhibited an obvious enhanced anti-oxidation ability. Whereas, both hydrothermal and solid-state reaction samples would be fully oxidized to V_2O_5 with continuously heating at 300 ℃ in air, in agreement with previous report [42].

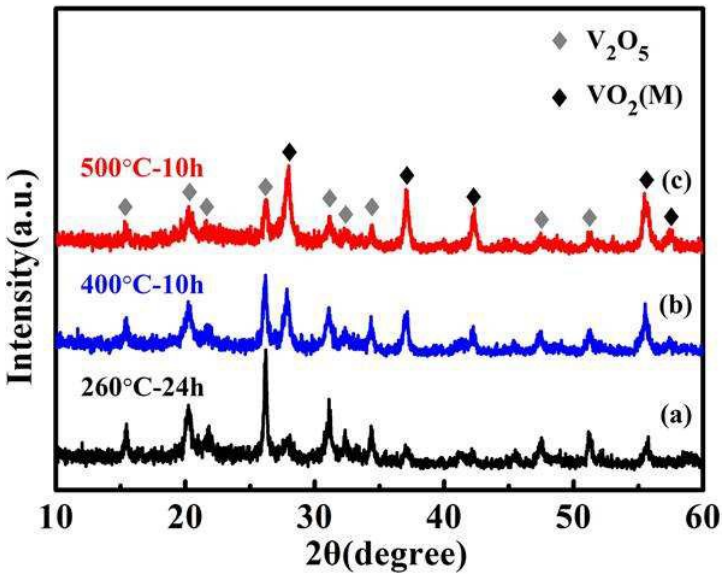

Figure 8 The XRD patterns of samples after heat treatment at 300 ℃ in air for 30 min (a, b, c). Samples of (a) were obtained via hydrothermal process (260 ℃ -24h) and the other were obtained in this work: (b) 400 ℃ -10h; (c) for 500 ℃ -10h.

As shown in Figure 9, the acid-corrosion experiment was carried out to test the acid-resistance ability of VO_2 (M1/R) NPs. Equal amount of VO_2 (M1/R) NPs (0.05g) obtained by hydrothermal and solid-state reaction were added to a hydrochloric acid solution (pH=1, 20 ml) at room temperature. The pH value of 1 was selected to accelerate erosion, but the dissolution was quite slow even under this pH value, therefore, a certain time of ultrasonic treatment (about 2 min) was employed to speed up the dispersion and corrosion rate for easier observation in a short time. It could be seen from Figure 9a that sample 2 of hydrothermal process immediately began to dissolve after ultrasonic treatment, and the solution appeared to be limpid with light

blue colour of VO^{2+} after a quite short duration time of 5 min (Figure 9b). In comparison, in the initial 1 min, sample 3 of this work exhibited no obvious changes compared with sample 1, and the blue colour of VO^{2+} was finally observed after 30 min. The relatively slow dissolution rate of VO_2 (M1/R) NPs of this work might be attributed to the slow reaction rate of large particles with other chemicals.

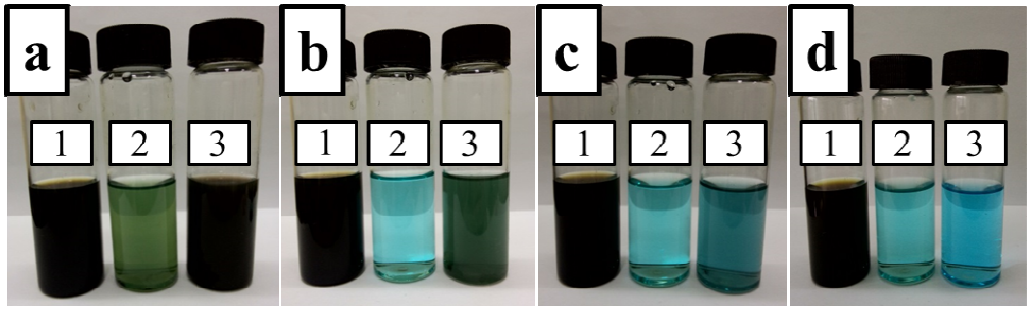

Figure 9 Photographs of VO_2 (M1/R) nanoparticles in deionized water (sample 1) and 0.1 M hydrochloric acid (sample 2, 3) at room temperature for different durations: (a) 1 min, (b) 5 min,(c) 10 min, and (d) 30 min. VO_2 (M1/R) NPs of sample 1 and sample 2 were both obtained via hydrothermal process (260 ºC -24h), and sample 3 for VO_2 (M1/R) nanoparticles obtained via solid-state reaction (500 ºC -10h).

From the aforementioned discussion, one can learn that VO_2 (M1/R) NPs prepared by the current solid-state-reaction process showed advantages in achieving enhanced performance. Firstly, a wide range of phase transition temperatures (from 43.5 °C to 59.3 °C) was achieved without using usual methods such as doping (which was widely used in various preparation processes[43-45]). Secondly, the optical properties (T_{lum} =54.2 % , ΔT_{sol} =9.2 %) of this work were comparable with those of W-doped films (T_{lum} =60.6 % , ΔT_{sol} =10.3 %)[43], nanoporous films (T_{lum} =50 % , ΔT_{sol} =14.7 %)[19], and F-doped composite foils (T_{lum} =45 % , ΔT_{sol} =10.8 %)[40]. Besides, the VO_2 (M1/R) NPs in this work showed enhanced chemical stability, thus improved the endurance of derived VO_2-based foils for practical usage[20]. In spite of the above advantages, there was still a problem with the low value of ΔT_{sol}, when compared with the excellent performance (22.3%)[25] in previous research of hydrothermal method, and the value of ΔT_{sol} needs to be improved to approach the calculated value (27%)[46] for smart window applications.

Conclusions

In summary, a solid-state reaction route was proposed to prepare well-crystallized VO_2 (M1/R) NPs with low, variable phase transition temperature, enhanced chemical stability and excellent thermochromic properties. The DSC results demonstrated that the phase transition temperatures ranged from 43.5 ℃ to 59.3 ℃ by regulating reaction conditions. The XRD, SEM and TEM analyses were made to study the growth of VO_2 (M1/R) NPs during the solid-state reaction, and it could be inferred that the amorphous phases around the crystalline VO_2 phases played an important role in the decrease of phase transition temperatures compared with the reported values (68 °C). Moreover, the obtained VO_2 (M1/R) NPs exhibited enhanced anti-oxidation and acid-resistance abilities compared with particles prepared by hydrothermal process, and the derived foils from the prepared VO_2 (M1/R) NPs also showed excellent thermochromic properties (T_{lum} =54.2 % , ΔT_{sol} =9.2 %). We believe that this synthetic strategy based on solid-state reaction, which could also be combined with various methods to improve optical properties, can significantly enrich the preparation techniques of VO_2 (M1/R) NPs and make great influence on practical applications of VO_2 (M1/R).

Acknowledgements

This study was supported in part by funds from MOST (2014AA032802), NSFC (State Outstanding Young Scholars, 51325203) and Shanghai Municipal Commission of Science and Technology (13521102100).

References

1. H. C. Wang, X. J. Yi and Y. Li, *Opt Commun*, 2005, **256**, 305-309.
2. A. Joushaghani, J. Jeong, S. Paradis, D. Alain, J. Stewart Aitchison and J. K. Poon, *Opt Express*, 2015, **23**, 3657-3668.
3. I. Balberg and S. Trokman, *J Appl Phys*, 1975, **46**, 2111-2119.
4. S. Sengupta, K. V. Wang, K. Liu, A. K. Bhat, S. Dhara, J. Q. Wu and M. M. Deshmukh, *Appl Phys Lett*, 2011, **99**, 062114.
5. Y. Gao, C. Cao, L. Dai, H. Luo, M. Kanehira, Y. Ding and Z. L. Wang, *Energ Environ Sci*,

2012, **5**, 8708-8715.

6. J. Zhou, Y. Gao, Z. Zhang, H. Luo, C. Cao, Z. Chen, L. Dai and X. Liu, *Sci Rep-Uk*, 2013, **3**, 3029.
7. Y. Gao, S. Wang, L. Kang, Z. Chen, J. Du, X. Liu, H. Luo and M. Kanehira, *Energ Environ Sci*, 2012, **5**, 8234-8237.
8. R. Binions, C. Piccirillo, R. G. Palgrave and I. P. Parkin, *Chemical Vapor Deposition*, 2008, **14**, 33-39.
9. M. E. A. Warwick, A. J. Roberts, R. C. T. Slade and R. Binions, *J Mater Chem A*, 2014, **2**, 6115-6120.
10. J. C. Orlianges, J. Leroy, A. Crunteanu, R. Mayet, P. Carles and C. Champeaux, *Appl Phys Lett*, 2012, **101**, 133102.
11. B. D. Ngom, M. Chaker, A. Diallo, I. G. Madiba, S. Khamlich, N. Manyala, O. Nemraoui, R. Madjoe, A. C. Beye and M. Maaza, *Acta Mater*, 2014, **65**, 32-41.
12. C. Ba, S. T. Bah, M. D'Auteuil, P. V. Ashrit and R. Vallee, *Acs Applied Materials & Interfaces*, 2013, **5**, 12520-12525.
13. Z. Huang, S. Chen, C. Lv, Y. Huang and J. Lai, *Appl Phys Lett*, 2012, **101**, 191905.
14. S. Kittiwatanakul, J. Laverock, D. Newby, K. E. Smith, S. A. Wolf and J. Lu, *J Appl Phys*, 2013, **114**, 053703.
15. D. Vernardou, M. E. Pemble and D. W. Sheel, *Chemical Vapor Deposition*, 2006, **12**, 263-274.
16. S. Fan, L. Fan, Q. Li, J. Liu and B. Ye, *Applied Surface Science*, 2014, **321**, 464-468.
17. S. Lee, C. Cheng, H. Guo, K. Hippalgaonkar, K. Wang, J. Suh, K. Liu and J. Wu, *J Am Chem Soc*, 2013, **135**, 4850-4855.
18. R. Binions, G. Hyett, C. Piccirillo and I. P. Parkin, *Journal Of Materials Chemistry*, 2007, **17**, 4652-4660.
19. X. Cao, N. Wang, J. Y. Law, S. C. Loo, S. Magdassi and Y. Long, *Langmuir*, 2014, **30**, 1710-1715.
20. L. Zhao, L. Miao, C. Liu, C. Li, T. Asaka, Y. Kang, Y. Iwamoto, S. Tanemura, H. Gu and H. Su, *Scientific reports*, 2014, **4**, 7000.
21. L. T. Kang, Y. F. Gao and H. J. Luo, *Acs Applied Materials & Interfaces*, 2009, **1**, 2211-2218.
22. C. X. Cao, Y. F. Gao and H. J. Luo, *Journal Of Physical Chemistry C*, 2008, **112**, 18810-18814.
23. L. Whittaker, T.-L. Wu, C. J. Patridge, G. Sambandamurthy and S. Banerjee, *Journal Of Materials Chemistry*, 2011, **21**, 5580-5592.
24. C. J. L. Whittaker, Z. G. Fu, D. A. Fischer, S. Banerjee, *Journal of the American Chemical Society*, 2009, **131**, 8884-8894.
25. Z. Chen, Y. Gao, L. Kang, C. Cao, S. Chen and H. Luo, *J Mater Chem A*, 2014, **2**, 2718-2727.
26. S. Chen, L. Dai, J. Liu, Y. Gao, X. Liu, Z. Chen, J. Zhou, C. Cao, P. Han, H. Luo and M. Kanahira, *Phys Chem Chem Phys*, 2013, **15**, 17537-17543.
27. N. Shen, S. Chen, Z. Chen, X. Liu, C. Cao, B. Dong, H. Luo, J. Liu and Y. Gao, *Journal of Materials Chemistry A*, 2014, **2**, 15087-15093.
28. J. D. Zhou, Y. F. Gao, X. L. Liu, Z. Chen, L. Dai, C. X. Cao, H. J. Luo, M. Kanahira, C. Sun and L. M. Yan, *Phys Chem Chem Phys*, 2013, **15**, 7505-7511.
29. S. R. Popuri, M. Miclau, A. Artemenko, C. Labrugere, A. Villesuzanne and M. Pollet, *Inorganic chemistry*, 2013, **52**, 4780-4785.

30. M. Li, X. Wu, L. Li, Y. Wang, D. Li, J. Pan, S. Li, L. Sun and G. Li, *J Mater Chem A*, 2014, **2**, 4520–4523.
31. C. Z. Wu, F. Feng, J. Feng, J. Dai, J. L. Yang and Y. Xie, *Journal Of Physical Chemistry C*, 2011, **115**, 791-799.
32. Y. Gao, S. Wang, H. Luo, L. Dai, C. Cao, Y. Liu, Z. Chen and M. Kanehira, *Energ Environ Sci*, 2012, **5**, 6104-6110.
33. M. Demeter , M. Neumann, W. Reichelt , *Surf Sci*, 2000, **454–456**, 41–44
34. J. C. Rakotoniaina, R. Mokranitamellin, J. R. Gavarri, G. Vacquier, A. Casalot and G. Calvarin, *J Solid State Chem*, 1993, **103**, 81-94.
35. J. Du, Y. F. Gao, H. J. Luo, L. T. Kang, Z. T. Zhang, Z. Chen and C. X. Cao, *Solar Energy Materials And Solar Cells*, 2011, **95**, 469-475.
36. H. Guo, K. Chen, Y. Oh, K. Wang, C. Dejoie, S. A. Syed Asif, O. L. Warren, Z. W. Shan, J. Wu and A. M. Minor, *Nano Lett*, 2011, **11**, 3207-3213.
37. M. J. Miller and J. Wang, *Journal of Applied Physics*, 2015, **117**, 034307.
38. J. Jeong, N. Aetukuri, T. Graf, T. D. Schladt, M. G. Samant and S. S. P. Parkin, *Science*, 2013, **339**, 1402-1405.
39. L. Kang, L. Xie, Z. Chen, Y. Gao, X. Liu, Y. Yang and W. Liang, *Applied Surface Science*, 2014, **311**, 676-683.
40. L. Dai, S. Chen, J. Liu, Y. Gao, J. Zhou, Z. Chen, C. Cao, H. Luo and M. Kanehira, *Phys Chem Chem Phys*, 2013, **15**, 11723-11729.
41. C. Liu, N. Wang and Y. Long, *Applied Surface Science*, 2013, **283**, 222-226.
42. G. Fu, A. Polity, N. Volbers and B. K. Meyer, *Thin Solid Films*, 2006, **515**, 2519-2522.
43. R. Chen, L. Miao, h. cheng, N. Eiji, C. Liu, A. Toru, Y. Iwamoto, M. Takata and S. Tanemura, *J. Mater. Chem. A*, 2015, **3**, 3726–3738
44. D. Li, M. Li, J. Pan, Y. Luo, H. Wu, Y. Zhang and G. Li, *ACS applied materials & interfaces*, 2014, **6**, 6555-6561
45. A. B. Huang, Y. J. Zhou, Y. M. Li, S. D. Ji, H. J. Luo and P. Jin, *J Mater Chem A*, 2013, **1**, 12545-12552.
46. S. Y. Li, G. A. Niklasson and C. G. Granqvist, *J Appl Phys*, 2010, **108**. 063525.

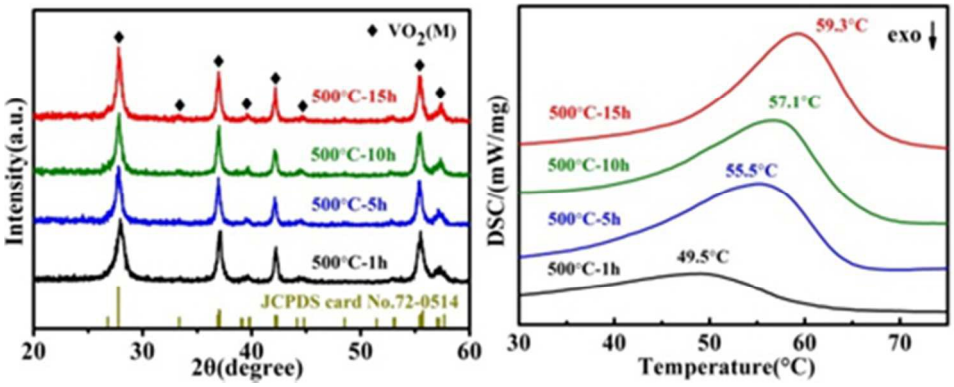

80x32mm (150 x 150 DPI)